Dengue virus cell entry

Ayala Nunez, Vanesa

Seeing is believing: how antibodies alter the cell entry pathway of dengue virus particles in living macrophages

Chapter 4

N.V. Ayala-Nunez[a], T. Hoornweg[a], D. van de Pol[a], K.A. Sjollema[b], H. van der Schaar[c], J.M. Smit[a*]

[a] Dept. of Medical Microbiology, University of Groningen, University Medical Center Groningen, Groningen, The Netherlands
[b] Dept. of Cell Biology, University of Groningen, University Medical Center Groningen, Groningen, The Netherlands
[c] Dept. of Infectious Diseases & Immunology, Virology Division, Faculty of Veterinary Medicine, Utrecht University, Utrecht, The Netherlands

Submitted

4

Abstract

Antibody-dependent enhancement (ADE) of dengue virus (DENV) infection is believed to play an important role in dengue-induced severe disease. Recent studies unraveled that both mature and immature DENV particles contribute to ADE. To understand how antibodies influence the fate of DENV particles, we explored the cell entry pathway of DENV with and without antibodies in macrophage-like cells. We showed that Ab-DENV predominantly enters through a phagocytosis-like pathway that involves a novel mechanism of initial virus-cell contact. This contact was facilitated by actin-mediated membrane protrusions that 1) engulf particles already bound to the cell, 2) capture virus particles localized away from the cell body, and 3) mediate virus uptake by non-directed ruffling of the cell membrane. Fusion was seen within Rab7 organelles. Overall, similar results were observed for standard and immature DENV preparations. Collectively, our findings suggest an unknown antibody-mediated mechanism that controls the cell entry pathway of DENV in macrophages.

Introduction

Dengue is the most common arthropod-borne viral infection in humans. There are five dengue virus serotypes (DENV1-5) and these cause around 390 million human infections worldwide each year[1, 2]. Approximately 500,000 to 1,000,000 individuals develop severe disease, presenting symptoms like plasma leakage, fluid accumulation, respiratory distress, severe bleeding, and organ impairment[3, 4]. Intriguingly, severe dengue is predominantly seen during primary infection in infants born to dengue-immune mothers and in individuals experiencing a heterologous secondary DENV infection[5-8]. These observations indicate that pre-existing antibodies are a risk factor for severe disease and led to the well-known hypothesis of antibody-dependent enhancement (ADE) of DENV infection[7, 9-11]. It is hypothesized that pre-existing cross-reactive DENV antibodies positively influence the infectious properties of the virus[7, 10]. As a consequence, the total infected cell mass increases and this triggers an imbalanced immune response leading to severe disease[10]. It is, however, not completely understood how the antibodies influence DENV infectivity.

DENV infectivity is mediated by the envelope (E) glycoprotein and involves three important steps: receptor binding, internalization into the host cell and membrane fusion[12, 13]. In the absence of antibodies, DENV E can bind to the cell by interacting with a wide range of receptor molecules, like DC-SIGN[14] or sulfated glycosaminoglycans (GAGs)[15]. Upon virus-receptor binding, DENV particles are predominantly internalized into the cell via clathrin-mediated endocytosis[16-18]. Membrane fusion typically occurs from within late endosomes, where low pH and anionic lipids trigger conformational changes in the E glycoprotein to mediate membrane fusion[16, 19]. DENV infects a variety of human cells, but cells of the monocyte lineage, like macrophages and dendritic cells, are considered the major target cells for DENV replication[10, 20].

DENV infectivity is controlled by the viral precursor membrane protein (prM)[21-24]. Within infected cells, prM has been shown to stabilize the E protein thereby preventing premature conformational changes within E during transit through the acidic Trans-Golgi network (TGN)[21]. Prior to the release of progeny virions, prM is cleaved into M and a pr peptide. DENV-infected cells are, however, known to secrete a very heterogeneous population of particles, ranging from mature M-containing viruses to fully immature prM-containing viruses[23]. Mature virions are considered to represent the infectious form of the virus. Fully immature particles, on the other hand, are essentially non-infectious in cells[21, 22]. Indeed, structural studies revealed that the pr peptide covers the E glycoprotein, thereby preventing binding and entry of immature virions into cells[25, 26]. The threshold of prM cleavage that is required for infectivity is currently unknown.

Interestingly, antibodies have been observed to stimulate infectivity of both mature and immature virions, indicating that all particles are likely to contribute to ADE of DENV infection[27-32]. Enhancement is seen when the antibody concentration

falls below the threshold required for virus neutralization[33]. During infection, DENV-antibody complexes are targeted to Fc-γ-receptor (FcγR) bearing cells. The antibody-FcγR interaction subsequently facilitates a more efficient binding and internalization of the virus into the cell[34, 35]. Indeed, the role of FcγRs in ADE has been confirmed *in vitro* and *in vivo*[29, 32, 36, 37]. Furthermore, the infectivity of antibody-opsonized immature DENV was found to be dependent on cellular furin activity, suggesting that immature virions mature upon virus entry[29]. An early study suggested that antibody-opsonized virions enter the cell via phagocytosis[34]. This was based on the observation that the internalization rate of antibody-opsonized virions resembled the rate of phagocytosis in macrophages[28, 34]. However, no details are known about the exact cell entry route of antibody-opsonized DENV in FcγR-bearing cells.

In this study, we unraveled how antibodies influence the cell entry pathway of DENV particles, thereby increasing our knowledge on the phenomenon of ADE. The route of DENV entry in the absence and presence of antibodies was analyzed in macrophages by (*i*) studying the dynamics of viral entry with single-particle tracking, (*ii*) examining the effect of a variety of endocytic chemical inhibitors on viral fusion, (*iii*) imaging – in real time – the interaction of the actin cytoskeleton with fluorescently labeled single virus particles, and (*iv*) exploring the Ab-DENV intracellular pathway by using Rab mutants. Furthermore, to address the role of prM on virus cell entry, we used both antibody-opsonized mature and immature DENV particles.

4

Results

Dynamics of antibody-mediated DENV cell entry

Antibody-mediated cell entry of DENV was investigated by use of human monoclonal antibodies mAb 5 and mAb 3-147, which recognize the E and prM protein respectively[30]. Standard DENV (stdDENV) was produced on C6/36 mosquito cells and immature DENV (prMDENV) was cultivated on furin-deficient LoVo cells[22]. The immature status of LoVo-derived DENV was confirmed by Western-blot analysis ([22], data not shown). The PFU-to-particle ratio of prMDENV was 7×10^7 ($\pm 2.5 \times 10^7$), which is 1,000,000 to 100,000-fold reduced compared to that of stdDENV. This is in line with previous studies[22, 29] and shows that prMDENV is essentially non-infectious in cells. After the initial characterization of the virus preparations, we determined the enhancing profile of the mAbs on murine macrophage-like P388D1 cells. We used P388D1 cells since they express FcγRIII (CD16), FcγRII (CD32), and FcγRI (CD64)[38, 39] and are known to support ADE of DENV[32, 40-42]. Murine FcγRs are considered to be structurally related to human FcγRs[43], hence, human antibodies are recognized by P388D1 cells. Prior to infection, mAb5 was complexed to stdDENV and mAb-3-147 was incubated with

prMDENV. Maximum enhancement of stdDENV infection (2 $\log_{10}$ increase in titers compared to the positive control) was obtained at a mAb concentration of 40 and 400 ng/mL (Fig. S1-A). In case of mAb 3-147, optimal ADE of prMDENV was reached at 0.1 ng/mL (Fig. S1-B). Furthermore, and in agreement with previous studies [22], we found that prMDENV is non-infectious in macrophage cells in the absence of antibodies (Fig. S1-B). Also, a considerable reduction of Ab-stdDENV (90% ± 3.7) and Ab-prMDENV (77.7% ± 1.2) infectivity was seen in cells treated with anti-CD16/CD32, confirming the importance of FcγRs in antibody-mediated cell entry (Fig. S1-C).

Then, we performed single virus tracking to investigate if antibodies influence the dynamics of viral entry. Single DENV particles were visualized by DiD labeling, as described before[16]. The infectivity of DiD-labeled DENV was comparable to that of unlabeled virus, indicating that the incorporation of the probe did not influence the functional properties of the virus (data not shown).

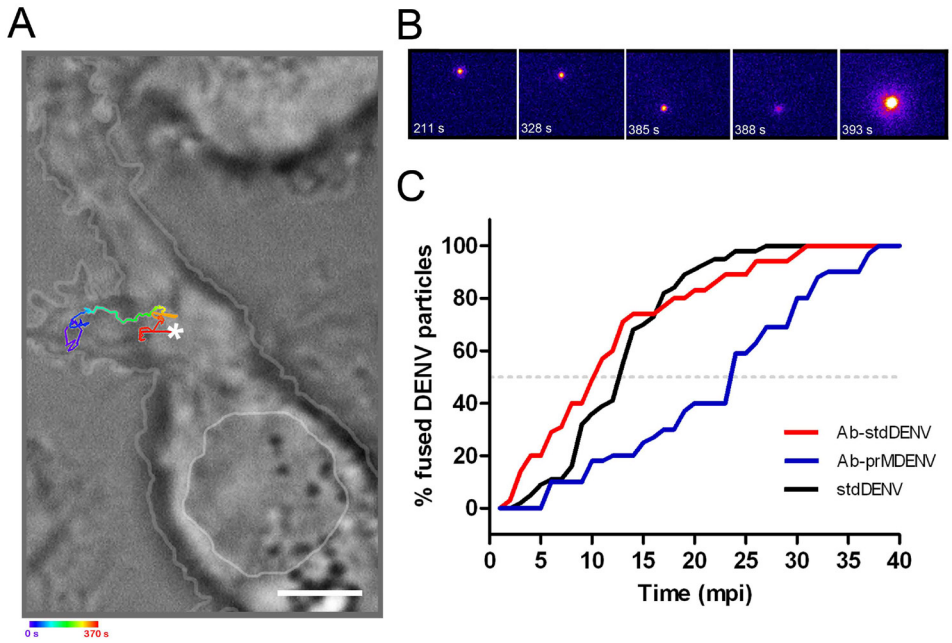

Figure 1. Kinetics of antibody-opsonized DENV entry in macrophages. Single-particle tracking of DiD-labeled Ab-stdDENV, Ab-prMDENV and stdDENV was performed in P388D1 cells at 1 frame per second. **(A)** Cell image obtained with DIC optics showing a trajectory of a single DiD-labeled Ab-stdDENV particle. The white star represents the membrane fusion site. Scale bar: 2 μm. **(B)** Snapshots of a DiD-labeled Ab-stdDENV particle at different time points post-infection. Membrane fusion is observed as a sudden increase in fluorescence intensity. The image was artificially modified to show the differences in fluorescence intensity, from low (purple) to high (yellow) intensity. **(C)** The percentage of fused virus particles calculated as a function of time. In total 35 trajectories were analyzed for Ab-stdDENV, 37 for Ab-prMDENV, and 36 for stdDENV. The time point of membrane fusion was defined as the moment when the DiD intensity doubles.

Upon DiD labeling, the virions were incubated with the previously defined enhancing concentrations of antibody and added to P388D1 cells. Subsequently, single-particle tracking of the DiD-labeled virus was performed at a time-lapse of 1 frame per second (37˚C). More than 50 movies were recorded. Figure 1A gives an example of a complete trajectory of an Ab-stdDENV particle in a P388D1 cell. Initially, this particle moves within the cell periphery, and then a rapid movement (likely on microtubules) is observed which is followed by intermitted movement prior to membrane fusion. The representative movie of this trajectory is uploaded as Movie S1. Quantification of the trafficking behavior was not possible as only a limited number of complete trajectories were recorded. In a large number of movies, parts of the trajectory are out of focus due to the thickness of macrophage cells. The specific time point of membrane fusion was defined as the moment when fluorescence intensity at least doubled. In the trajectory of Figure 1B, fusion is seen at 393 seconds post-addition of the stdDENV-immune complex to the cell. Quantitative analysis revealed a considerable delay in the fusion time point of Ab-prMDENV with respect to Ab-stdDENV and stdDENV (Fig. 1C). As illustrated in Figure 1C, 50% of the Ab-prMDENV particles have fused within 24 min. On the other hand, however, 50% fusion of Ab-stdDENV particles was seen at 10 min, which indicates that prM influences the dynamics of viral entry. Furthermore, an intermediate time point (13 min) of fusion was detected for stdDENV in the absence of antibodies.

Analyzing DENV cell entry by chemical inhibitors

The differences in fusion time points may reflect the usage of different entry pathways. This prompted us to further evaluate the cell entry pathway of DENV in the absence and presence of antibodies. To define the cell entry pathway, various perturbants of endocytic pathways were added to the cells. The concentration of the chemical inhibitors used was defined based on successful inhibition of entry of known fluorescently labeled cargo controls, like transferrin, dextran and cholera toxin B (see Fig. S2). The effect of the compound on DENV cell entry was measured by use of a fluorescence microscopy-based fusion assay. We have used this assay before and quantified viral internalization by measuring the extent of fusion of DiD-labeled virus[44]. Interestingly, as can also be deduced from Figure 2A (left column upper and bottom image), enhanced DENV membrane fusion activity is seen in presence of enhancing concentration of antibodies. Subsequent quantification of the fluorescence intensity of 15 randomly selected images derived from three independent experiments revealed that membrane fusion activity of Ab-stdDENV is 6-fold increased compared to that of stdDENV. This indicates that ADE indeed involves enhanced cell entry and/or membrane fusion of DENV particles.

To further validate the assay used, cells were infected in presence of FcγR blocker or ammonium chloride (NH_4Cl), a compound known to neutralize

the pH of intracellular compartments. As seen in Figure 2, the FcγR blocker markedly reduced the membrane fusion capacity of DiD-labeled stdDENV and prMDENV particles in the presence of enhancing concentrations of antibodies. These observations are in line with the results obtained in the titration assay and confirm that antibody-mediated entry of DENV in P388D1 cells is mediated by FcγRs. As expected, no membrane fusion was seen in cells treated with NH_4Cl (Fig. 2A-C). All of the above results are in line with the literature[29, 34, 45] and demonstrate that the microscope assay can be used to evaluate the route of antibody-mediated DENV cell entry.

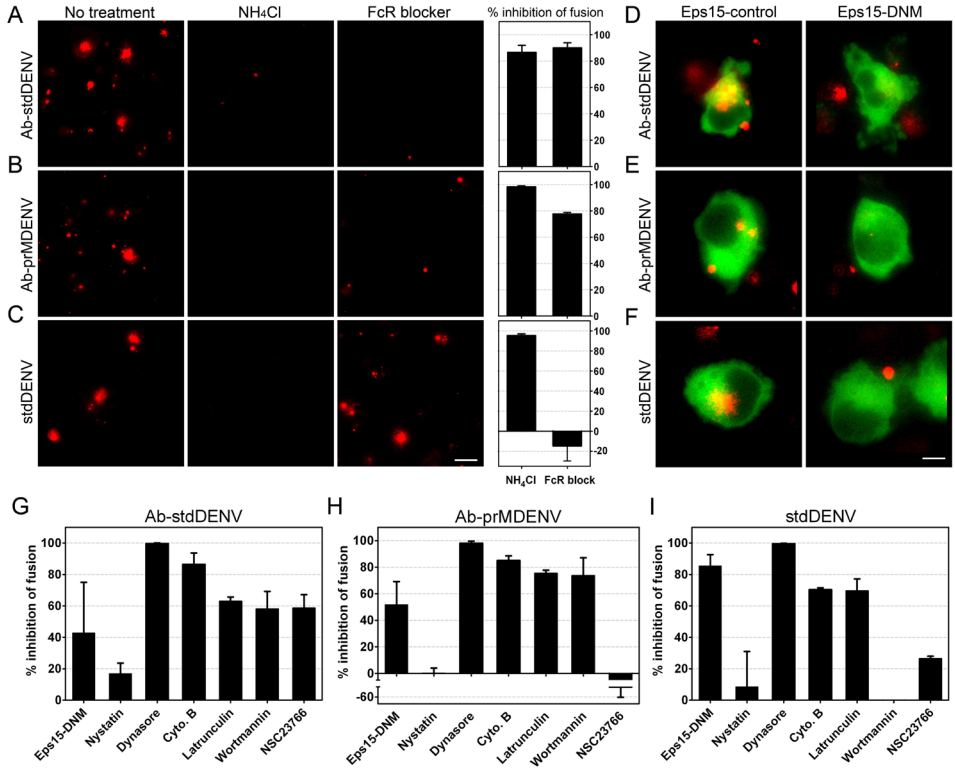

Figure 2. Antibody-opsonized DENV entry inhibition by endocytic inhibitors. DiD-labeled DENV (opsonized and non-opsonized) was added *in situ* to P388D1 cells in the presence or absence of the indicated inhibitors. After 30 min of infection at 37°C, the cells were washed and snapshots were taken with an oil-immersion 100x objective. **(A-C)** Representative images upon DiD-DENV infection with and without prior treatment of the cells with NH_4Cl (50 mM) and FcR blocker are shown. Scale bar: 25 μm. Fusion inhibition was calculated by analyzing the total extent of membrane fusion of DiD-labeled virus with ImageJ. **(D-F)** Representative images of a fusion assay performed in P388D1 cells electroporated with Eps15-GFP (empty vector D3Δ2 (control) and DNM (E95/295)). Scale bar: 7 μm. **(G-I)** Fusion inhibition of different biochemical inhibitors with an end concentration of 50 μM nystatin, 150 μM dynasore, 15 μM cytochalasine B, 1 μM latrunculin, 2 μM wortmannin, or 250 μM NSC23766 was used. The percentage of fusion inhibition was calculated with respect to the non-treated control. The average of at least three independent experiments is shown ± SEM.

We started to investigate the route of cell entry by examining the role of clathrin and caveolae in antibody-mediated DENV cell entry. We first tested a

dominant negative mutant (DNM) of Eps15 (E95/295), a protein required for clathrin-dependent uptake[46]. As seen in Figure 2D-F, the Eps15-DNM inhibited fusion in all three infection conditions, albeit to a different extent. The most extensive inhibition (>80%) was seen following infection with stdDENV in the absence of antibodies (Fig. 2F and I). These results point towards a role of the clathrin machinery in entry of DENV and antibody-bound DENV. Treatment of cells with nystatin, a cholesterol binding agent, leads to a complete ablation of morphologically identifiable caveolae[47]. We observed that nystatin treatment had no influence on stdDENV, Ab-stdDENV or Ab-prMDENV fusion (Fig. 2G-I), which suggests that entry of DENV with and without Abs is caveolae-independent.

Thereafter, the role of dynamin and actin was measured. Dynamin, a small GTPase, has a critical role in endocytic membrane fission events[48]. Actin is important in numerous endocytic pathways, like clathrin-mediated endocytosis[49], macropinocytosis[50], caveolae-mediated endocytosis[51], and phagocytosis[52]. Though the actin cytoskeleton function is variable between distinct endocytic pathways[53]. Treatment of P388D1 cells with dynasore, a compound that interferes with the GTPase activity of dynamin1 and dynamin2[54], abolished membrane fusion activity of DENV irrespective of the maturation status and with and without prior opsonization with antibodies (Fig. 2G-I). Moreover, disruption of actin filaments with cytochalasin B and latrunculin was found to reduce fusion of Ab-stdDENV, Ab-prMDENV and stdDENV (Fig. 2G-I). Inhibition of PI3K, a key coordinator in actin remodeling, through wortmannin, also reduced membrane fusion activity of Ab-stdDENV and Ab-prMDENV (Fig. 2 G-I). However, inhibition of Rac1 (NSC23766), a Rho GTPase involved in controlling actin cytoskeleton organization, blocked Ab-stdDENV but not Ab-prMDENV membrane fusion (Fig. 2G-H). Wortmannin and NSC23766 had little effect on stdDENV fusion (Fig. 2I). These results demonstrate that actin and the regulators of actin remodeling play a critical role during Ab-DENV endocytosis. The different response to PI3K inhibitors is consistent with a distinct DENV cell entry mechanism in the presence and absence of antibodies.

Ab-DENV activates extensive ruffling of the cell membrane via FcγRs

The actin cytoskeleton has been observed to support different processes related to endocytosis, like the invagination of membrane segments into the cytoplasm, elongation of invaginations, and protrusions in the form of filopodia and ruffles[52, 55]. In order to study how antibody-opsonized DENV particles interact with the actin cytoskeleton, we performed live-cell imaging in eYFP-actin expressing P388D1 cells. Interestingly, dramatic changes in cell morphology and actin redistribution were observed upon infection with DiD-labeled Ab-stdDENV and Ab-prMDENV (Fig. 3). Ab-stdDENV and Ab-prMDENV particles were not only seen at the cell surface (3A), but also associated with membrane ruffles (3B) and

filopodia-like structures (3C). Ruffles were observed across the cell membrane as sheet-like protrusive structures with a heterogeneous morphology (Fig. 3D).

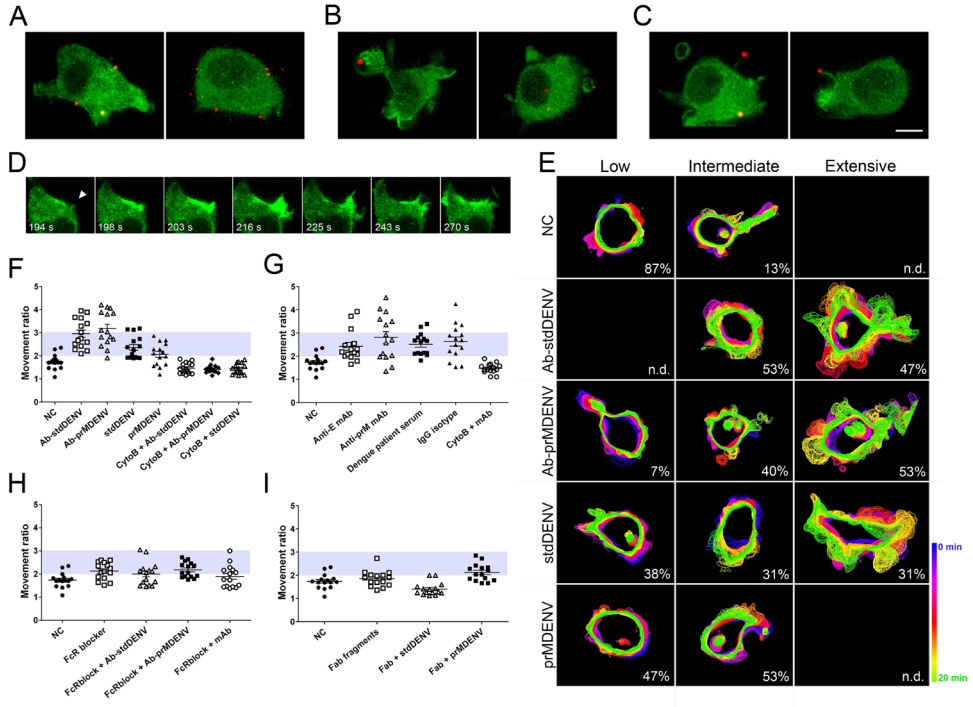

Figure 3. Ab-DENV induction of actin cytoskeleton rearrangement via FcγRs. DiD-labeled virus (Ab-stdDENV, Ab-prMDENV and stdDENV) was added to eYFPActin-expressing P388D1 cells. The cells were kept at 37°C for live-cell imaging with a spinning disk confocal microscope. Ab-DENV was observed to localize to the **(A)** cell membrane, **(B)** membrane ruffles and **(C)** actin filopodia during entry. Scale bar: 7 μm. **(D)** Time series of antibody-opsonized DENV induced cell membrane ruffling. The white arrowhead indicates the place where the ruffle starts. **(E-I)** Cell movement was quantified over time upon the indicated treatments. **(E)** Representative images of P388D1 cells under the indicated conditions are shown as the overlays of the cell body outlines of a time-lapse of 20 min. **(F-I)** The Movement ratio (MR) quantifies the extent of movement of one cell over a frame sequence. See Figure S3 for more details on how to calculate it. Based on the MR, the movement response was classified as Low (MR < 2), Intermediate (MR = 2-3) or Extensive (MR > 3). For each condition, 15 cells were used for analysis. The gray area indicates the intermediate response. The proportion of cells showing Low, Intermediate, and Extensive response is indicated at the right corner of **(E)**.

The extensive actin-driven membrane ruffling is illustrated by Movies S2 and S3. In the absence of any added stimuli (negative control), the eYFP-Actin expressing macrophages are constitutively active (as reported by [56]), but do not show widespread ruffling of the membrane (Movie S4). Ruffling induced by Ab-stdDENV and Ab-prMDENV is initiated at 3 to 5 minutes post-infection (mpi) (Movies S5 and S6). Movie S5 shows eYFP-Actin expressing cells during the first 4.5 minutes following infection with Ab-stdDENV. DiD-labeled particles are visible, but not yet bound to the cell membrane. A constitutive movement of the cell body can be seen. Movie S6 shows the same group of cells at 5 mpi. A widespread and highly active ruffling of the cells is evident.

But what is triggering membrane ruffling? Is it the immune complex, the virus or the antibody? To address this issue, we first developed an ImageJ-based method to quantify the extent of cell ruffling in one cell. With this method, we calculated the "Movement ratio" (MR) by dividing the "total area" covered by a moving cell for the whole sequence, with respect to the smallest surface area occupied by the same cell in the same time series (explained in detail in Fig. S3). Based on the resulting Movement ratio, cells were classified in three groups: Low (MR < 2), Intermediate (MR = 2-3), and Extensive (MR > 3). To visually illustrate the results, the projections of the cell body outlines of a time-lapse of 20 min are shown in Figure 3E. No differences were observed between the ruffling response activated by Ab-stdDENV (Movie S2) and Ab-prMDENV (Movie S3). Extensive membrane ruffling is observed in approximately 50% of the cells infected with Ab-stdDENV (47%) and Ab-prMDENV (53%) (Fig. 3E-F). Cells infected with stdDENV and prMDENV in the absence of antibodies predominantly show intermediate ruffling, 31% and 53% respectively (Fig. 3E-F). Cytochalasin B prevented membrane ruffling in all conditions (MR < 2). The addition of soluble anti-E and anti-prM antibodies to the cells also induced membrane ruffling, albeit to a somewhat lower extent than antibody-opsonized DENV (Fig. 3G). Similar results were found upon addition of dengue patient immune serum and an IgG isotype antibody. Collectively, these results indicate that membrane ruffling is not caused by the virus but is triggered through the addition of antibodies to cells.

These results prompted us to further study the role of antibodies in ruffling induction of the cell membrane. The use of a FcγR blocker (anti-CD16/CD32) prevented ruffling induced by Ab-stdDENV, Ab-prMDENV and by soluble anti-E mAbs (Fig. 3H). In addition, we observed that Fab fragments with and without prior opsonization to stdDENV and prMDENV particles do not induce extensive ruffling (Fig. 3I). Taken together, these results indicate that activation of membrane ruffling in macrophages by Ab-stdDENV and Ab-prMDENV is likely triggered through the interaction of the antibody with a FcγR expressed at the cell surface.

Ruffling involvement in Ab-DENV internalization

Ruffling, the involvement of actin, and the role of PI3K suggests that cell entry of antibody-opsonized DENV may take place via macropinocytosis, as has been recently shown for several other viruses (for reviews see [57] and [58]). Macropinocytosis is an actin-dependent process characterized by the formation of macropinosomes, which are structures of eukaryotic plasma membranes ranging in size from 0.2 to 10 μm that are used to engulf extracellular fluid for cellular uptake[59]. Indeed, upon infection with Ab-stdDENV and Ab-prMDENV, membrane ruffles were seen that close to form macropinosomes (Movies S7 and S8). In Figure 4A, a time series of the closure of a vesicle is presented. Actin accumulation is visible in the area of ruffle formation and in the newly formed macropinosome.

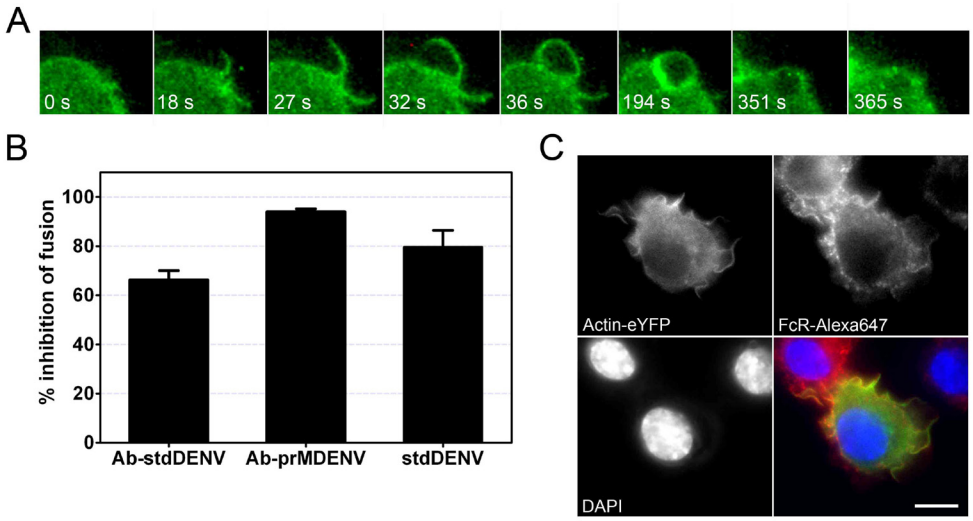

Figure 4. Role of antibody-induced macropinocytosis in virus internalization. (A) Time series showing the formation and internalization of a macropinosome **(B)** P388D1 cells were treated with EIPA (100 μM) for 1 h at 37°C. Cells were infected with DiD-labeled Ab-stdDENV, Ab-prMDENV and stdDENV and analyzed as in Figure 2. **(C)** FcγR expression in eYFPActin-expressing cells. Scale bar: 10 μm.

Macropinosome formation requires Na^+/H^+ exchanger (NHE) activity to modulate Rho GTPases at the cytoplasmic membrane[60]. Inhibition of NHE activity by EIPA (an amiloride derivative), is often used to define the role of macropinocytosis in a specific process[60]. In our case, EIPA treatment indeed blocked Ab-stdDENV, Ab-prMDENV and stdDENV fusion in P388D1 cells (Fig. 4B). However, caution should be taken because NHEs can also be found in the membrane of other intracellular vesicles[61], thereby potentially interfering with other pH-dependent endocytic pathways as well.

Taken together, our findings indicate that antibodies induce macropinocytosis over a large fraction of the cellular plasma membrane by extensive actin-mediated ruffle formation. As the consequence of this cell-wide activation, viral particles may be internalized through macropinosomes[58]. Since antibody-mediated entry of DENV is facilitated through interaction with FcγRs, we wondered whether we could detect these receptors in ruffles. Figure 4C shows that FcγRs are widely expressed on ruffles induced by Ab-stdDENV, thereby potentially explaining the mechanism of binding and uptake through macropinocytosis. However, uptake through macropinocytosis appears to be rather inefficient as only a few macropinosomes contained visible Ab-stdDENV (4 out of 50) or Ab-prMDENV (2 out of 50) complexes.

Ab-opsonized DENV is internalized by actin cell-surface protrusions

Given the inefficient uptake of virus particles by macropinocytosis, we questioned whether we could also detect other types of viral uptake in macrophages.

Indeed, upon further analysis of the recorded movies, we also observed viral uptake through localized cell-surface actin protrusions (Fig. 5). These were not considered as part of the ruffling response described in the previous section, since ruffling was observed as a general response of the complete cell body and these protrusions represent localized reactions to a viral particle.

We observed two distinct types of localized actin-mediated uptake of Ab-DENV. Type 1 implies uptake through actin protrusions that are formed upon direct virus-cell contact (Fig. 5A). In case of Type 2, actin protrusions were generated towards viral particles located away from the cell body. Once the actin-mediated structure reached the virus particle, the filopodia retracts and pulls back the virion to the cell membrane (Fig. 5C and Movie S9).

To evaluate the efficiency of these processes we quantified the number of events by visual examination. Type 1 and Type 2 virus-cell interactions were counted in 73 cells per condition and classified as successful or unsuccessful, based on the ability of the actin protrusion to mediate viral uptake. In total, 60 events (including both Type 1 and 2) were recorded for Ab-stdDENV, 31 events for Ab-prMDENV, and 29 events for stdDENV. Representative examples are shown in Figure 5A-D. Figure 5A shows a successful Type I uptake. The antibody-opsonized DiD-labeled particle is bound to the plasma membrane. At 2.6 mpi, an actin protrusion starts to surround the virus particle and subsequently captures it. Figure 5B shows an unsuccessful Type 1 uptake. This particle is surrounded by actin protrusions but did not end up inside a cellular compartment. A successful Type 2 uptake is illustrated in Figure 5C. Initially, an antibody-opsonized virus is seen approximately 5 μm away from the cell body. Then, a filopodia-like structure protrudes and elongates in the direction of the virus particle. This protrusion reaches and binds to the viral particle, and pulls it back to the cell body. The complete process lasts 54 seconds. This is also visible in Movie S9. Figure 5D presents an unsuccessful Type 2 uptake. Here, actin protrusions are directed towards the virion but fail to pull it back. Since we observed Type 2 taking place multiple times against the same particle (Movie S10), we believe that Type 2 movement represents a specific direct process to capture virus particles from the extracellular environment. In all conditions, Type 1 appears to be more efficient than Type 2 (Fig. 5E-G). The frequency of successful Type 1 uptake is similar for Ab-stdDENV, Ab-prMDENV and stdDENV (Fig. 5E-G). Successful Type 2 uptake was seen in 8 out of 36 (22%) events for Ab-stDENV and 4 out of 11 (36%) for Ab-prMDENV (Fig. 5E-F).

Type 2 is, however, a remarkable phenomenon that seems to play an active role in antibody-mediated uptake. As observed in Figure 5C, Type 2 uptake is directed specifically against a single virus particle that is not moving and not associated with the plasma membrane or any other visible actin structure. But how is the cell able to sense the presence and position of the virus without having contact with it? Or is the membrane surface area of the cells wider than seen by eYFP-actin? To address this issue, we stained the membranes of eYFP-Actin expressing cells with

the lipophilic probe DiD and used high resolution differential interference contrast (DIC) microscopy to evaluate the membrane surface area of the cells. The DiD signal completely overlaps with eYFP-actin, indicating that all cellular structures are detected with eYFP-Actin (Fig. S4). At this moment we do not know how cells sense the virions. Interestingly, though, Type 2 interactions were only observed in case of antibody-opsonized stdDENV and prMDENV and not in the absence of antibodies (Fig. 5G).

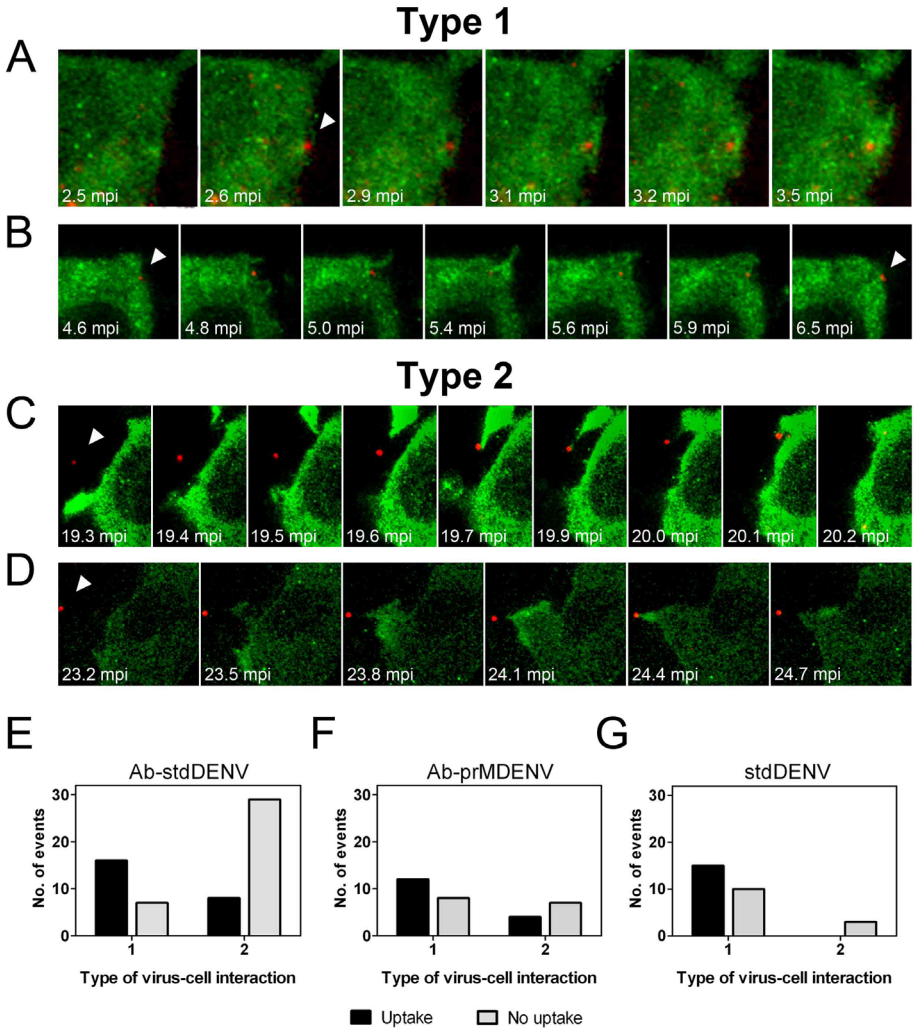

Figure 5. Ab-DENV uptake is mediated by actin protrusions. The experimental set-up is similar as described in the legend to Figure 3. **(A-D)** Representative montages of alternating time-lapse exposures of DiD-DENV and eYFPActin during entry. **(A-B)** Type 1 virus uptake. **(C-D)** Type 2 virus uptake. DiD-virus is shown in red. eYFPActin expressing cells are shown in green. White arrowheads point out single viral particles associated with actin structures. **(E-G)** Frequency of Type 1 and type 2 uptake in a total of 60 events.

Endocytic trafficking of antibody-opsonized DENV

After uptake and internalization, most viruses traffic through intracellular vesicles till a compartment is reached where membrane fusion occurs (refer to [62] for an extensive review). The intracellular compartments hijacked by viruses can be endosomes, phagosomes or pinosomes, all of which have been described to undergo acidification and a maturation process that involves the gain and loss of early/late markers before fusion with lysosomes[57, 63, 64]. Since trafficking of the different intracellular compartments is controlled by Rab GTPases[65], we used a set of fluorescently-labeled Rab dominant-negative mutants (DNM) to analyze which of these GTPases is required for viral transport. Fluorescently labeled dextran was used as a control to evaluate the activity of the DNMs. Fig. S2 shows that the overexpression of Rab5 and Rab7 DNMs inhibited uptake of the fluorescently-labeled dextran. DENV membrane fusion activity was reduced in cells transfected with DNM of Rab7 for all experimental conditions (Fig. 6A-C), particularly in the case of stdDENV in the absence of antibodies (88% of inhibition with respect to the WT Rab7). Interestingly, Rab5 was required for Ab-DENV fusion (black bars, Fig. 6D-F), but not for stdDENV.

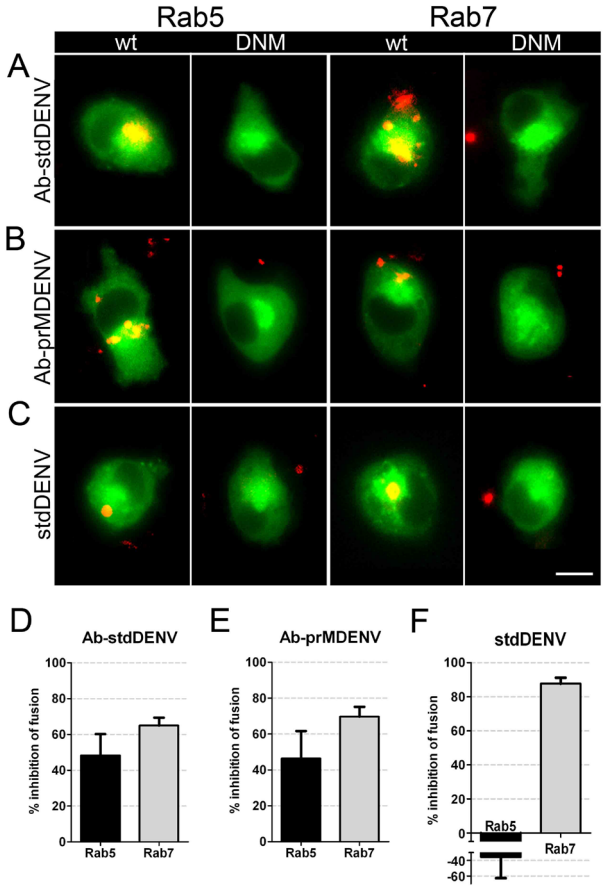

Figure 6. Effect of Rab5 and Rab7 dominant-negative mutants in fusion of Ab-DENV. DiD-labeled DENV (with and without antibodies) was added *in situ* to P388D1 cells electroporated with the indicated plasmids. **(A-C)** Representative examples of membrane fusion. Membrane fusion of DiD-labeled virus is observed as highly fluorescent red puncta in the WT and DNM electroporated cells. All plasmids have GFP as a reporter gene. Scale bar: 7 μm. **(C)** Quantification of the effect of the DNM proteins on viral fusion. For analysis, 85 cells positive for the expression of the plasmids were used. The percentage of inhibition was calculated with respect to the WT plasmid control.

Discussion

The study presented here aimed to understand how DENV enters macrophages in the absence and presence of antibodies. A model with our main findings on DENV entry is shown in Figure 7. In brief, actin rearrangements in the form of cell surface protrusions actively mediate internalization. For DENV infection in the absence of antibody, only Type 1 and 3 are observed. For antibody-opsonized stdDENV/prMDENV, Types 1, 2 and 3 are seen. Engulfment occurs when the viral particles are enclosed by filopodia-like structures or membrane ruffles. Distinct entry pathways are used by DENV in the absence and presence of antibodies. Antibody-mediated entry was found to be FcγR, pH, clathrin, dynamin, actin, PI3K, Rab5, and Rab7-dependent, but caveolae-independent. DENV cell entry in the absence of antibodies is pH, clathrin, dynamin, actin, and Rab7-dependent, but FcγR, caveolae, PI3K, and Rab5-independent.

The biochemical signature of DENV entry in the absence of antibodies does not fit with a classical textbook view of one endocytic process. The importance of clathrin and dynamin is suggestive for entry via clathrin-mediated endocytosis[46]. The actin cytoskeleton is important in numerous endocytic and phagocytic processes, but the function of actin within these processes is different[55]. In classical clathrin-mediated endocytosis, actin supports the process of invagination of the membrane and helps with the elongation and scission of the new vesicle[55]. We, however, observed that actin forms active membrane protrusions that engulf the particles (Type 1), a phenomenon that has been linked to phagocytic processes[66]. Entry through phagocytosis seems unlikely, however, since PI3K is not required in DENV cell entry and this molecule is generally believed to be important for phagosomal maturation[66, 67]. Therefore, we propose that DENV entry in macrophages is via a novel mechanism involving elements of different entry pathways. Furthermore, enhanced membrane fusion was seen in Rab5-DNM expressing cells whereas a marked inhibition was noticed in Rab7-DNM cells. This suggests that DENV particles bypass Rab5 organelles and are immediately delivered to Rab7 compartments were membrane fusion occurs. Similar results were observed for lymphocytic choriomeningitis virus[68]. The authors suggested that this atypical transport behavior may serve to internalize plasma membrane molecules and bound ligands that need to avoid recycling regulated by Rab5 early endosomes[68]. The observation that DENV fuses from within Rab7 compartments is in agreement with our earlier data[16] and is in line with the described lipid dependence for DENV fusion[19].

The entry profile of antibody-opsonized DENV is similar to stdDENV entry except for the role of FcγRs and PI3K. On the basis of this difference we propose that antibody-opsonized DENV entry in macrophages occurs through a phagocytosis-like pathway. Indeed, FcγRs[66], dynamin[69], active formation of actin protrusions[52, 66], and PI3K[70] have been linked to phagocytosis. We also observed involvement of the clathrin machinery in Ab-DENV internalization. This is in line with entry through

phagocytosis as different elements of the clathrin machinery, like AP-2, have been located in the outer layer of phagosomes and play a role in phagosomal maturation[71, 72]. Phagocytosis-like entry may seem unexpected given the relatively small size of Ab-DENV complexes. Indeed, it is generally believed that phagocytosis is meant for uptake of particles larger than 0.5 μm[66]. Yet, phagocytosis-like pathways have been described for viruses with smaller dimensions, like Adenovirus type 2 (90-100 nm)[73] and HSV-1 (200 nm)[74]. Hence, the size of the particles is not the only determinant needed to trigger phagocytosis[74]. Upon phagocytosis, the antibody-opsonized particles traffic through Rab5 and Rab7 organelles and both early and late phagosomes are required for entry and membrane fusion in P388D1 macrophages. Given the pH and lipid requirements for fusion, we anticipate that the virus predominantly fuses from within late phagosomal compartments.

A surprising novel finding was Type 2 uptake of antibody-opsonized stdDENV and prMDENV. To our knowledge, this is the first study that describes the possibility of a cell to actively search and capture a virus particle from the environment. But how is the cell able to detect virus particles located away from its main body? A possible explanation is chemotaxis. Antibodies are known to associate and dissociate from their antigen over time[75]. It is tempting to speculate that the dissociated antibodies leak away from the complex and serve as a chemotactic stimulus that macrophages can sense. Indeed, Type 2 uptake was not observed with stdDENV in the absence of antibodies. Thus, antibodies not only flag the virus as a foreign antigen that needs to be degraded, they may also induce an active capturing mechanism in macrophage cells. In this sense, Type 2 is a remarkable example of how viruses could utilize pathogen-sensing functions of macrophages.

Macropinocytosis may serve as a parallel entry pathway for both antibody-opsonized and non-opsonized DENV into macrophages. Cell entry through macropinocytosis is reported for a growing number of viruses, like poxviruses, filoviruses, influenza A virus (IAV), adenovirus and human immunodeficiency virus (HIV)[76-81]. However, in the case of DENV, only very few viral particles were seen inside pinosomes, suggesting this is not the main route of entry. What then is the role of the extensive membrane ruffling that is observed following the addition of antibodies or Ab-DENV particles? Activation of extensive macropinocytosis in macrophages may be considered a host defense strategy as it (*i*) allows bulk internalization of nutrients from the environment, which would provide the cell the required energy to adequately respond to danger signals like foreign material or antibodies, (*ii*) avoids the silencing of inflammatory responses observed in some phagocytic-mediated processes, (*iii*) provides the macrophage with an alternative to clear large amounts of extracellular material, which cannot be done with phagocytosis. Simultaneously, the virus may take advantage of this phenomenon and use the enhanced nutrient uptake for virus replication. Indeed, macropinocytosis was observed to positively influence the multiplication of the bacteria *Brucella abortus*[82].

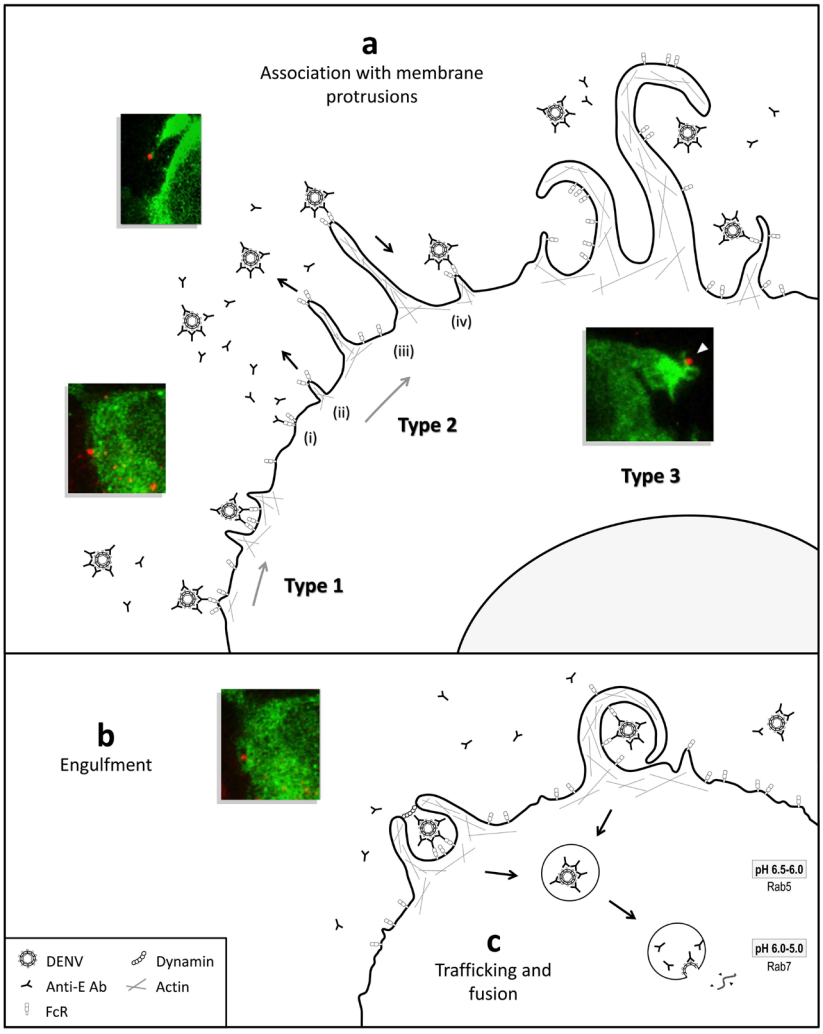

Figure 7. Model of DENV entry into macrophages. The model illustrates the major steps involved in stdDENV, Ab-stdDENV, and Ab-prMDENV entry in macrophage-like cells. The fluorescence microscopy images provide examples for each step. For clarity purposes, only drawings with Ab-opsonized stdDENV particles are shown. In brief, the infection of macrophage-like cells starts with **(a)** the association with membrane protrusions: Type 1, Ab-stdDENV directly binds to FcγRs at the cell membrane; Type 2, virus particles are detected by the cell and pulled back by membrane protrusions; Type 3, virions associate with membrane ruffles expressing FcγRs. All 3 modes of uptake are seen for Ab-stdDENV and Ab-prMDENV, whereas only Types 1 and 3 are observed for stdDENV in the absence of antibodies. It is as yet unknown which receptor facilitates Type 1 and 3 uptake following DENV infection in the absence of antibodies. **(b)** Engulfment occurs when Ab-DENV is surrounded by actin protrusions to form a phagocytic cup. In case of the macropinocytosis-like uptake, Ab-DENV is engulfed by ruffles that close to form a pinosome. **(c)** Trafficking of Ab-DENV takes place via Rab5 compartments. The antibody-opsonized virus primarily fuses within Rab7 compartments.

We observed that the fusion time point of DiD-labeled Ab-prMDENV particles is approximately two times delayed compared to Ab-stdDENV. This observation points to a distinct trafficking behavior of Ab-prMDENV particles in cells. Previous studies showed that immature DENV has to undergo a furin-

dependent maturation process prior to membrane fusion[29]. It is known that progeny virions release the pr peptide upon secretion of the particle to the extracellular pH neutral milieu[25]. During infection, it is hypothesized that the lower pH of late phagosomal compartments –when compared to the luminal pH of vesicles within the Golgi apparatus– is sufficient to release the pr peptide from the virion[26]. Hence, we postulate that the additional time required to initiate membrane fusion reflects the processes involved in virion maturation.

It is important to mention that an antibody-mediated entry pathway by itself does not entirely explain ADE. Under neutralizing conditions, virions will also enter macrophages via an antibody-mediated pathway. Indeed, FcγRs have been shown to be important in antibody-mediated neutralization as well as antibody-mediated enhancement of infection[34, 41, 83, 84]. Hence, it is likely that a similar entry pathway is used under neutralizing and enhancing conditions. What then determines the enhancing or neutralizing capacity of the antibody? We and others have suggested that ADE is controlled at the level of membrane fusion[36, 85]. Fusion and thus ADE may occur when antibodies dissociate from the virion during entry or bind with low occupancy thereby allowing unoccupied E proteins to undergo fusion. Furthermore, prM antibodies are likely to dissociate from the virion when the pr peptide is released and therefore these antibodies are preferentially linked to ADE.

In conclusion, our results provide evidence for a novel antibody-mediated mechanism meant to regulate the uptake and internalization of DENV particles in macrophages. The overall pattern of Ab-stdDENV and Ab-prMDENV was similar, indicating that the antibody dictates the route of entry and not the virion. This data not only elucidates how antibodies alter the cell entry pathway of DENV particles in living macrophages, but also shows that Ab-virus complexes can take advantage of an active pathogen-sensing mechanism of macrophages. It would be interesting to establish whether the intervention of these entry pathways may be useful in the design of antiviral drugs that can be used in dengue severe disease.

Experimental procedures

Cells and viruses

Murine macrophage P388D1 cells were maintained in DMEM (PAA) supplemented with 10% FBS, penicillin (100 U/mL), streptomycin (100 µg/mL), sodium bicarbonate (Invitrogen, 7.5% solution) and 1.0 mM sodium pyruvate (Gibco). Baby hamster kidney (BHK-15) cells were cultured in 1x high glucose, L-glutamine-enriched DMEM with 10% FBS, penicillin (100 U/mL), and streptomycin (100 µg/mL). *Aedes albopictus* C6/36 cells were maintained in MEM (Gibco) supplemented with 10% FBS, 25 mM HEPES, 7.5% sodium bicarbonate, penicillin (100 U/mL), streptomycin (100 µg/mL), 200 mM glutamine and 100 µM nonessential amino acids at 30˚C. Human adenocarcinoma (LoVo) cells were cultured in Ham's F-12 medium

(Gibco) supplemented with 20% FBS, penicillin (100 U/mL), and streptomycin (100 µg/mL). All cells except for C6/36 were maintained at 37°C and 5% CO_2.

Standard DENV2 strain 16681 was kindly provided by Dr. Claire Huang (Center for Disease Control and Prevention, USA). It was propagated in C6/36 cells as described before[22]. Immature (prM) DENV2 particles were produced in LoVo cells, as described previously[86]. Viral infectivity was determined by plaque assay on BHK-15 cells (plaque forming units, PFU)[86]. The absolute number of virus particles in solution was determined by quantitative PCR (qPCR), which detects the number of genome-containing particles (GCPs)[29]. Virus infection was performed on the basis of multiplicity of genome-containing particles per cell (MOG).

Antibodies

Human anti-E (mAb 5) and anti-prM (mAb 3-147) monoclonal antibodies were kindly provided by Gavin Screaton (Imperial College, London, UK). Purified anti-Mouse CD16/CD32 (Mouse BD Fc Block) was obtained from BD Biosciences. Convalescent human dengue immune serum (28 days following DENV2 infection) was generously provided by Dr. G. Comach (Biomed-UC, Lardidev, Maracay, Venezuela) and Dr. T. Kochel (U.S. Naval Medical Research Center Detachment, Lima, Peru). Mouse IgG2A Isotype Control (anti-KLH) was acquired from R&D Systems. Fab fragments were made from the monoclonal murine anti-E antibody 4G2 (Millipore) by use of the Pierce™ Fab Micro Preparation Kit.

Drugs and reagents

Endocytotic inhibitors such as colchicine, wortmannin, nystatin, dynasore, cytochalasin B, and latrunculin were purchased from Sigma Aldrich. Ammonium chloride (NH_4Cl) was obtained from Merck and the Rac1 selective inhibitor NSC23766 from Tocris Bioscience. A furin-specific inhibitor, decanoyl-L-arginyl-L-valyl-L-lysyl-L-arginyl-chloromethylketone (decRRVKR-CMK), was obtained from Calbiochem. The fluorescently labeled endocytic cargos Cholera toxin B-FITC (CtxB-FITC), Dextran-FITC, Dextran-TxRd, and Lysotracker Green were purchased from Life Technologies.

Plasmids

The GFP-tagged dominant-negative Eps15 mutant E95/295 and its empty vector D3Δ2 were kindly provided by Dr. A. Benmerah and Dr. A. Dautry-Varsat (Institute Pasteur, Paris, France). The eYFP-Actin construct (human β-actin in a pCDNA3.1 vector) was obtained from Dr. Ben Giepmans (UMCG, Groningen, The Netherlands). The Rab5-S34N-GFP dominant negative mutant (DNM) and Rab5-wt-GFP plasmids were generously provided by Dr. P. van der Sluijs (University Medical Center, Utrecht, The Netherlands). The Rab7-T22N-GFP DNM and Rab7-wt-GFP plasmids were obtained from Gary R. Whittaker (Cornell University College of Veterinary Medicine, NY, USA).

ADE assay

For virus-antibody complex formation, virus particles (MOG 1000 of std as well as prMDENV) were incubated for 30 min at 37˚C in presence of serial 10-fold dilutions of antibodies in cell culture medium containing 2% FBS. The virus-antibody complexes were then added to 2 × 10^5 P388D1 cells/well, and incubated at 37˚C with 5% CO_2. At 43 hours post-infection, the supernatant was collected and virus particle production was measured with a plaque assay. As a control, an FcR blocker (anti-mouse CD16/CD32) was used. The cells were pretreated with the FcR blocker (1 μg per 1 x 10^6 cells) for 10 min at 4˚C before infection.

DiD-labeling of DENV

The lipophilic fluorescent probe 1,1'-dioctadecyl-3,3,3',3'-tetramethylindodicarbocyanine, 4-chlorobenzenesulfonate salt (DiD) (Molecular Probes) was used to label the viral membrane of DENV virus particles, as previously described[87, 88]. When incorporated in the viral membrane at a relatively high surface density, the emitted fluorescence level is largely quenched, but single DiD-labeled virus particles can still be clearly detected. Membrane fusion is detected as an increase in fluorescence intensity due to dilution of the probe into the target membrane

ADE assays for DENV fusion and infection

DiD-labeled std DENV was incubated with 400 ng/mL of mAb 5 and DiD-labeled prMDENV with 1 ng/mL of mAb 3-147 prior to the addition to P388D1 cells seeded in an 8-wells Lab-Tek II Chambered Coverglass (Nunc). Cells were then incubated for 30 min at 37˚C with 5% CO_2. The extent of membrane fusion of the DiD virus was determined with a fusion assay as described before[88]. Briefly, the P388D1 cells were washed three times and a microscopy analysis was done by taking 15 snapshots of randomly selected fields using both differential interference contrast (DIC) and DiD channels. DiD-labeled viruses were detected by epi-fluorescence microscopy in a Leica Biosystems 6000B instrument by using a 635-nm helium–neon laser. The acquired images were processed and analyzed with ImageJ using an in-house macro. The extent of membrane fusion was quantified by measuring the total fluorescent signal per field of view with the "Particle analyzer" plugin of ImageJ. The percentage of fusion inhibition was calculated with respect to the non-treated positive control.

Single-particle tracking of DiD-DENV

The tracking experiments were performed as previously described[87]. Briefly, P388D1 cells were seeded in 8-wells Lab-Tek II Chambered Coverglass two days before infection. Prior to the experiment, cells were washed three times with phenol red-free MEM and warm phenol red-free MEM containing 1% glucose was added. DiD-labeled DENV (opsonized or non-opsonized std and prMDENV) was added

to P388D1 cells at 37°C and kept at the same temperature throughout the tracking experiment. DiD-labeled DENV was detected with a 633-nm helium-neon laser. Image series of the fluorescent emission were recorded with a charge-coupled-device camera at 1 frame per s. Before and after fluorescence imaging, the localization of the nucleus and plasma membrane of the cell was determined by use of DIC optics. The acquired images were processed and analyzed with ImageJ and Imaris x64 7.6.1. Only those virus particles that showed more than a two-fold increase in fluorescence intensity after membrane fusion were used for single-particle tracking analysis. Trajectories were generated by pairing peaks in each frame to previously established trajectories according to proximity and similarity in intensity.

Drug inhibitor studies with DiD-DENV

Multiple endocytic inhibitors were used to define the route of DENV entry. The effect of the inhibitors on DENV infectivity was measured by use of a microscopic membrane fusion assay[88]. In brief, P388D1 cells were seeded in a Lab-Tek II Chambered Coverglass (Nunc No. 155409) two days before the infection. The cells were washed three times and treated with the drug of interest for 1.5 h at 37 °C (NH_4Cl, Latrunculin and EIPA treatments were done for 1 h). An end concentration of 50 mM NH_4Cl, 50 μM nystatin, 150 μM dynasore, 15 μM cytochalasine B, 1 μM latrunculin, 2 μM wortmannin, 250 μM NSC23766 or 100 μM EIPA was used. All drug dilutions were prepared in serum-free phenol red-free MEM (Gibco) containing 1% glucose and used at non-toxic concentrations. Then, DiD-labeled virus (stdDENV, Ab-stdDENV, or Ab-prMDENV) was added to the well in the presence of the compound at an MOG of 400. For virus-antibody complex formation, stdDENV and prMDENV were incubated for 30 min at 37°C with 400 ng/mL of mAb 5 or 10 ng/mL of mAb 3-147 in serum-free media, respectively. The cells were then incubated 30 min at 37°C to allow virus entry. This time-point was chosen since 90% of the particles have fused within this timeframe (Figure 1C). Then, a fusion assay was performed as described in previous sections. The percentage of fusion inhibition was calculated with respect to the non-treated positive control.

Electroporation of P388D1 cells

A suspension containing 3 x 10^6 cells (in antibiotic-free DMEM containing 10% FBS) and 10 μg of DNA plasmid were placed in a 0.4 cm electroporation cuvette (Bio-Rad). The electroporation was performed at room temperature, 950 μF and 250 V. Afterwards, the cuvette was kept at room temperature for 4 min. The cells were then resuspended and seeded in an 8-wells Lab-Tek using antibiotic-free 10% FBS DMEM. The media was refreshed one day after electroporation. The cells were used for imaging on days two and three post-electroporation.

Live-cell imaging in eYFP-Actin expressing cells

P388D1 cells were electroporated with the eYFP-Actin construct (10 μg of

DNA per $3x10^6$ cells) and seeded in an 8-wells Lab-Tek II Chambered Coverglass. At 2 days post-electroporation, the cells were washed with serum-free phenol red-free MEM and fresh serum-free phenol red-free 1% glucose MEM was added to the well. Then, DiD-labeled virus (stdDENV or prMDENV) with and without prior antibody opsonization was added *in situ* in the presence or absence of the indicated treatments. The virus used for live-cell imaging was UV-inactivated for 1 h. UV-treatment did not interfere with membrane fusion activity (data not shown).

Living P388D1 cells electroporated with the eYFP-Actin construct were imaged with a Solamere Spinning Disk Confocal Live Cell Imaging system (Solamere Technology Group). This system is based on a confocal Leica DM IRE2 Inverted microscope (Leica Microsystems) equipped with a temperature and CO_2 controlled box (Live Imaging Services). YFP and DiD fluorescence were recorded with a Stanford Photonics XR/Mega-10 ICCD camera (Stanford Photonics) using argon (488 nm) and krypton (647 nm) lasers as light sources, respectively. Time-lapse acquisition was done at 1 image every 4.5 seconds with a 63x objective. The acquired images were processed and analyzed with Imaris x64 7.6.1 (Bitplane Scientific Software) and ImageJ (NIH).

Immunostaining of FcγRs in P388D1 cells

Cells electroporated with eYFP-Actin construct were grown to subconfluence in an 8-wells Lab-Tek II Chambered Coverglass in cell culture medium. Prior to infection, cells were washed with PBS. At 30 min post-infection, the P388D1 cells were fixed with 2% paraformaldehyde (in 40 mM HEPES buffer, pH 7.2, containing 6.8% sucrose) for 30 min at 37˚C. The fixed cells were immersed in 0.25% NH_4C1/PBS for 10 min at room temperature to quench free aldehyde. Subsequently, the cells were permeabilized with 0.1% Triton X-IO0-2% BSA in PBS for 5 min and immunostained. For detection of FcγR, anti-Mouse CD16/CD32 was used as a primary antibody and rabbit anti-mouse Alexa647 (Life Technologies) as a secondary antibody. DAPI was used for nuclei staining. FcγR expression in eYFP-Actin positive cells was assessed by epi-fluorescence microscopy in a Leica Biosystems 6000B instrument.

Dominant-negative mutant assays

DiD-labeled DENV was added *in situ* to P388D1 cells electroporated beforehand with the Eps15-GFP (DNM E95/295 and its empty vector D3Δ2) Rab5-GFP (DNM S34N and WT) and Rab7-GFP (T22N DNM and WT) plasmids. A fusion assay was performed as described in previous sections. To assess the effect of the DNM on membrane fusion of the virus, 85-100 cells positive for the expression of the plasmid (GFP+) were the extent of membrane fusion was quantified in these cells as described in previous sections. The percentage of inhibition of fusion of the DNM was calculated with respect to the WT plasmid control. Ammonium chloride (50 mM) was used as a negative control (data not shown).

Fluorescently labeled cargo controls for biochemical inhibitors and DNM

To confirm the inhibitory activity of the chemical inhibitors, different fluorescently labeled cargo controls were used. The activity of nystatin was confirmed by incubation of cells with CtxB-FITC for 30 min at 37˚C. Cells treated with colchicine, cytochalasin B, latrunculin, wortmannin, NSC23766, and EIPA were incubated with Dextran-FITC for 30 min at 37˚C to assess the inhibitory effect. To define the effect of ammonium chloride on the pH of acidic intracellular vesicles, P388D1 cells were stained with Lysotracker Green for 15 min at 37˚C, then washed twice with serum-free phenol red-free MEM. Visualization was done by use of an epi-fluorescence Leica Biosystems 6000B microscope.

The activity of the Rab5 and Rab7 DNM plasmids was confirmed with the use of Dextran-TxRd. P388D1 cells were electroporated with the Rab5 or Rab7 WT and DNM plasmids. Two days post-electroporation, the cells were treated with Dextran-TxRd (0.03 μg/mL) for 30 min at 37˚C, washed and then imaged to assess Dextran uptake or co-localization. Rab5 electroporated cells were visualized with an epi-fluorescence Leica Biosystems 6000B microscope. To assess the effect of the Rab5-DNM on uptake of Dextran, 50 cells positive for the expression of the plasmid (GFP+) were selected and scored as positive or negative for uptake. The percentage of inhibition of uptake of the DNM was calculated with respect to the WT plasmid control. On the other hand, the activity of the Rab7-DNM was defined by quantifying co-localization of Dextran molecules and Rab7-GFP+ compartments. Since expression of the DNM form of Rab7 blocks the exit of cargo molecules from early to late compartments[89], we quantified co-localization of Dextran molecules and with Rab7-WT and DNM compartments. To this end, the cells were fixed with PFA 4% and imaged with a Leica SP8 Confocal microscope. Fifty Dextran molecules were assessed per condition.

Acknowledgements

We thank Prof A. van Oijen and Dr. I.A. Rodenhuis-Zybert for fruitful discussions and valuable comments on the manuscript. This work was supported by the Dutch Organization for Scientific Research Division Earth and Life Sciences (granted to JMS). Part of the work was performed at the UMCG Microscopy and Imaging Center (UMIC).

References

1. D. Normile. **First New Dengue Virus Type in 50 Years**http://news.sciencemag.org/health/2013/10/first-new-dengue-virus-type-50-years.
2. Bhatt, S. *et al*. The global distribution and burden of dengue. *Nature* **496**, 504-507 (2013).
3. Gubler, D. J. Epidemic dengue/dengue hemorrhagic fever as a public health, social and economic problem in the 21st century. *Trends Microbiol.* **10**, 100-103 (2002).
4. World Health Organization. **Dengue guidelines for diagnosis, treatment, prevention and control: new edition**. (2009).
5. Halstead, S. B. Observations related to pathogensis of dengue hemorrhagic fever. VI. Hypotheses and discussion. *Yale J. Biol. Med.* **42**, 350-362 (1970).
6. Russell, P. K. *et al*. An insular outbreak of dengue hemorrhagic fever. II. Virologic and serologic studies. *Am. J. Trop. Med. Hyg.* **17**, 600-608 (1968).
7. Halstead, S. B. Immune enhancement of viral infection. *Prog. Allergy* **31**, 301-364 (1982).
8. Kliks, S. C., Nimmanitya, S., Nisalak, A. & Burke, D. S. Evidence that maternal dengue antibodies are important in the development of dengue hemorrhagic fever in infants. *Am. J. Trop. Med. Hyg.* **38**, 411-419 (1988).
9. Vaughn, D. W. *et al*. Dengue viremia titer, antibody response pattern, and virus serotype correlate with disease severity. *J. Infect. Dis.* **181**, 2-9 (2000).
10. Halstead, S. B. Dengue virus-mosquito interactions. *Annu. Rev. Entomol.* **53**, 273-291 (2008).
11. Rothman, A. L. Immunity to dengue virus: a tale of original antigenic sin and tropical cytokine storms. *Nat. Rev. Immunol.* **11**, 532-543 (2011).
12. Rey, F. A. Dengue virus envelope glycoprotein structure: new insight into its interactions during viral entry. *Proc. Natl. Acad. Sci. U. S. A.* **100**, 6899-6901 (2003).
13. Grove, J. & Marsh, M. The cell biology of receptor-mediated virus entry. *J. Cell Biol.* **195**, 1071-1082 (2011).
14. Alen, M. M. *et al*. Antiviral activity of carbohydrate-binding agents and the role of DC-SIGN in dengue virus infection. *Virology* **387**, 67-75 (2009).
15. Chen, Y. *et al*. Dengue virus infectivity depends on envelope protein binding to target cell heparan sulfate. *Nat. Med.* **3**, 866-871 (1997).
16. van der Schaar, H. M. *et al*. Dissecting the cell entry pathway of dengue virus by single-particle tracking in living cells. *PLoS Pathog.* **4**, e1000244 (2008).
17. Acosta, E. G., Castilla, V. & Damonte, E. B. Functional entry of dengue virus into Aedes albopictus mosquito cells is dependent on clathrin-mediated endocytosis. *J. Gen. Virol.* **89**, 474-484 (2008).
18. Suksanpaisan, L., Susantad, T. & Smith, D. R. Characterization of dengue virus entry into HepG2 cells. *J. Biomed. Sci.* **16**, 17 (2009).
19. Zaitseva, E., Yang, S. T., Melikov, K., Pourmal, S. & Chernomordik, L. V. Dengue virus ensures its fusion in late endosomes using compartment-specific lipids. *PLoS Pathog.* **6**, e1001131 (2010).
20. Halstead, S. B. Antibody, macrophages, dengue virus infection, shock, and hemorrhage: a pathogenetic cascade. *Rev. Infect. Dis.* **11 Suppl 4**, S830-9 (1989).
21. Li, L. *et al*. The flavivirus precursor membrane-envelope protein complex: structure and maturation. *Science* **319**, 1830-1834 (2008).
22. Zybert, I. A., van der Ende-Metselaar, H., Wilschut, J. & Smit, J. M. Functional importance of dengue virus maturation: infectious properties of immature virions. *J. Gen. Virol.* **89**, 3047-3051 (2008).
23. Junjhon, J. *et al*. Influence of pr-M cleavage on the heterogeneity of extracellular dengue virus particles. *J. Virol.* **84**, 8353-8358 (2010).
24. Pierson, T. C. & Diamond, M. S. Degrees of maturity: the complex structure and biology of flaviviruses. *Curr. Opin. Virol.* **2**, 168-175 (2012).
25. Yu, I. M. *et al*. Structure of the immature dengue virus at low pH primes proteolytic maturation. *Science* **319**, 1834-1837 (2008).
26. Zheng, A., Umashankar, M. & Kielian, M. In vitro and in vivo studies identify important features of dengue virus pr-E protein interactions. *PLoS Pathog.* **6**, e1001157 (2010).
27. Kliks, S. C., Nisalak, A., Brandt, W. E., Wahl, L. & Burke, D. S. Antibody-dependent enhancement of dengue virus growth in human monocytes as a risk factor for dengue hemorrhagic fever. *Am. J. Trop.*

Med. Hyg. **40**, 444-451 (1989).
28. Morens, D. M. & Halstead, S. B. Measurement of antibody-dependent infection enhancement of four dengue virus serotypes by monoclonal and polyclonal antibodies. *J. Gen. Virol.* **71 (Pt 12)**, 2909-2914 (1990).
29. Rodenhuis-Zybert, I. A. *et al*. Immature dengue virus: a veiled pathogen? *PLoS Pathog.* **6**, e1000718 (2010).
30. Dejnirattisai, W. *et al*. Cross-reacting antibodies enhance dengue virus infection in humans. *Science* **328**, 745-748 (2010).
31. Colpitts, T. M. *et al*. prM-antibody renders immature West Nile virus infectious in vivo. *J. Gen. Virol.* **92**, 2281-2285 (2011).
32. da Silva Voorham, J. M. *et al*. Antibodies against the envelope glycoprotein promote infectivity of immature dengue virus serotype 2. *PLoS One* **7**, e29957 (2012).
33. Pierson, T. C. *et al*. The stoichiometry of antibody-mediated neutralization and enhancement of West Nile virus infection. *Cell. Host Microbe* **1**, 135-145 (2007).
34. Halstead, S. B. & O'Rourke, E. J. Dengue viruses and mononuclear phagocytes. I. Infection enhancement by non-neutralizing antibody. *J. Exp. Med.* **146**, 201-217 (1977).
35. Gollins, S. W. & Porterfield, J. S. Flavivirus infection enhancement in macrophages: radioactive and biological studies on the effect of antibody on viral fate. *J. Gen. Virol.* **65 (Pt 8)**, 1261-1272 (1984).
36. Rodrigo, W. W., Jin, X., Blackley, S. D., Rose, R. C. & Schlesinger, J. J. Differential enhancement of dengue virus immune complex infectivity mediated by signaling-competent and signaling-incompetent human Fcgamma RIA (CD64) or FcgammaRIIA (CD32). *J. Virol.* **80**, 10128-10138 (2006).
37. Balsitis, S. J. *et al*. Lethal antibody enhancement of dengue disease in mice is prevented by Fc modification. *PLoS Pathog.* **6**, e1000790 (2010).
38. Sung, S. S. Phagocytosis by mouse peritoneal macrophages plated on monoclonal antibody-coated immune complex-substrates: effects of complexes of different IgG subclasses on Fc receptor functions. *J. Immunol.* **135**, 1981-1986 (1985).
39. Ochiai, H., Kurokawa, M., Hayashi, K. & Niwayama, S. Antibody-mediated growth of influenza A NWS virus in macrophagelike cell line P388D1. *J. Virol.* **62**, 20-26 (1988).
40. Halstead, S. B. *et al*. Comparison of P388D1 mouse macrophage cell line and human monocytes for assay of dengue-2 infection-enhancing antibodies. *Am. J. Trop. Med. Hyg.* **32**, 157-163 (1983).
41. Morens, D. M., Halstead, S. B. & Marchette, N. J. Profiles of antibody-dependent enhancement of dengue virus type 2 infection. *Microb. Pathog.* **3**, 231-237 (1987).
42. Huang, K. J. *et al*. The dual-specific binding of dengue virus and target cells for the antibody-dependent enhancement of dengue virus infection. *J. Immunol.* **176**, 2825-2832 (2006).
43. Haeffner-Cavaillon, N., Klein, M. & Dorrington, K. J. Studies on the Fc gamma receptor of the murine macrophage-like cell line P388D1. I. The binding of homologous and heterologous immunoglobulin G1. *J. Immunol.* **123**, 1905-1913 (1979).
44. Ayala-Nunez, N. V., Jarupathirun, P., Kaptein, S. J., Neyts, J. & Smit, J. M. Antibody-dependent enhancement of dengue virus infection is inhibited by SA-17, a doxorubicin derivative. *Antiviral Res.* **100**, 238-245 (2013).
45. Kuhn, R. J. *et al*. Structure of dengue virus: implications for flavivirus organization, maturation, and fusion. *Cell* **108**, 717-725 (2002).
46. McMahon, H. T. & Boucrot, E. Molecular mechanism and physiological functions of clathrin-mediated endocytosis. *Nat. Rev. Mol. Cell Biol.* **12**, 517-533 (2011).
47. Rothberg, K. G. *et al*. Caveolin, a protein component of caveolae membrane coats. *Cell* **68**, 673-682 (1992).
48. Ferguson, S. M. & De Camilli, P. Dynamin, a membrane-remodelling GTPase. *Nat. Rev. Mol. Cell Biol.* **13**, 75-88 (2012).
49. Kaksonen, M., Toret, C. P. & Drubin, D. G. Harnessing actin dynamics for clathrin-mediated endocytosis. *Nat. Rev. Mol. Cell Biol.* **7**, 404-414 (2006).
50. Lee, E. & Knecht, D. A. Visualization of actin dynamics during macropinocytosis and exocytosis. *Traffic* **3**, 186-192 (2002).
51. Mundy, D. I., Machleidt, T., Ying, Y. S., Anderson, R. G. & Bloom, G. S. Dual control of caveolar membrane traffic by microtubules and the actin cytoskeleton. *J. Cell. Sci.* **115**, 4327-4339 (2002).
52. May, R. C. & Machesky, L. M. Phagocytosis and the actin cytoskeleton. *J. Cell. Sci.* **114**, 1061-1077 (2001).
53. Girao, H., Geli, M. I. & Idrissi, F. Z. Actin in the endocytic pathway: from yeast to mammals. *FEBS Lett.* **582**, 2112-2119 (2008).
54. Macia, E. *et al*. Dynasore, a cell-permeable inhibitor of dynamin. *Dev. Cell.* **10**, 839-850

(2006).
55. Mooren, O. L., Galletta, B. J. & Cooper, J. A. Roles for actin assembly in endocytosis. *Annu. Rev. Biochem.* **81**, 661-686 (2012).
56. Flannagan, R. S., Harrison, R. E., Yip, C. M., Jaqaman, K. & Grinstein, S. Dynamic macrophage "probing" is required for the efficient capture of phagocytic targets. *J. Cell Biol.* **191**, 1205-1218 (2010).
57. Mercer, J. & Helenius, A. Virus entry by macropinocytosis. *Nat. Cell Biol.* **11**, 510-520 (2009).
58. Mercer, J. & Helenius, A. Gulping rather than sipping: macropinocytosis as a way of virus entry. *Curr. Opin. Microbiol.* **15**, 490-499 (2012).
59. Swanson, J. A. Shaping cups into phagosomes and macropinosomes. *Nat. Rev. Mol. Cell Biol.* **9**, 639-649 (2008).
60. Koivusalo, M. *et al*. Amiloride inhibits macropinocytosis by lowering submembranous pH and preventing Rac1 and Cdc42 signaling. *J. Cell Biol.* **188**, 547-563 (2010).
61. Lawrence, S. P., Bright, N. A., Luzio, J. P. & Bowers, K. The sodium/proton exchanger NHE8 regulates late endosomal morphology and function. *Mol. Biol. Cell* **21**, 3540-3551 (2010).
62. Mercer, J., Schelhaas, M. & Helenius, A. Virus entry by endocytosis. *Annu. Rev. Biochem.* **79**, 803-833 (2010).
63. Racoosin, E. L. & Swanson, J. A. Macropinosome maturation and fusion with tubular lysosomes in macrophages. *J. Cell Biol.* **121**, 1011-1020 (1993).
64. Kinchen, J. M. & Ravichandran, K. S. Phagosome maturation: going through the acid test. *Nat. Rev. Mol. Cell Biol.* **9**, 781-795 (2008).
65. Stenmark, H. Rab GTPases as coordinators of vesicle traffic. *Nat. Rev. Mol. Cell Biol.* **10**, 513-525 (2009).
66. Flannagan, R. S., Jaumouille, V. & Grinstein, S. The cell biology of phagocytosis. *Annu. Rev. Pathol.* **7**, 61-98 (2012).
67. Vieira, O. V. *et al*. Modulation of Rab5 and Rab7 recruitment to phagosomes by phosphatidylinositol 3-kinase. *Mol. Cell. Biol.* **23**, 2501-2514 (2003).
68. Quirin, K. *et al*. Lymphocytic choriomeningitis virus uses a novel endocytic pathway for infectious entry via late endosomes. *Virology* **378**, 21-33 (2008).
69. Huynh, K. K. & Grinstein, S. Phagocytosis: dynamin's dual role in phagosome biogenesis. *Curr. Biol.* **18**, R563-5 (2008).
70. Gillooly, D. J., Simonsen, A. & Stenmark, H. Phosphoinositides and phagocytosis. *J. Cell Biol.* **155**, 15-17 (2001).
71. Aggeler, J. & Werb, Z. Initial events during phagocytosis by macrophages viewed from outside and inside the cell: membrane-particle interactions and clathrin. *J. Cell Biol.* **94**, 613-623 (1982).
72. Chen, D. *et al*. Clathrin and AP2 are required for phagocytic receptor-mediated apoptotic cell clearance in Caenorhabditis elegans. *PLoS Genet.* **9**, e1003517 (2013).
73. Meier, O., Gastaldelli, M., Boucke, K., Hemmi, S. & Greber, U. F. Early steps of clathrin-mediated endocytosis involved in phagosomal escape of Fcgamma receptor-targeted adenovirus. *J. Virol.* **79**, 2604-2613 (2005).
74. Clement, C. *et al*. A novel role for phagocytosis-like uptake in herpes simplex virus entry. *J. Cell Biol.* **174**, 1009-1021 (2006).
75. Davies, D. R., Padlan, E. A. & Sheriff, S. Antibody-antigen complexes. *Annu. Rev. Biochem.* **59**, 439-473 (1990).
76. Schmidt, F. I., Bleck, C. K., Helenius, A. & Mercer, J. Vaccinia extracellular virions enter cells by macropinocytosis and acid-activated membrane rupture. *EMBO J.* **30**, 3647-3661 (2011).
77. Mercer, J. & Helenius, A. Vaccinia virus uses macropinocytosis and apoptotic mimicry to enter host cells. *Science* **320**, 531-535 (2008).
78. Hunt, C. L., Kolokoltsov, A. A., Davey, R. A. & Maury, W. The Tyro3 receptor kinase Axl enhances macropinocytosis of Zaire ebolavirus. *J. Virol.* **85**, 334-347 (2011).
79. Rossman, J. S., Leser, G. P. & Lamb, R. A. Filamentous influenza virus enters cells via macropinocytosis. *J. Virol.* **86**, 10950-10960 (2012).
80. Meier, O. *et al*. Adenovirus triggers macropinocytosis and endosomal leakage together with its clathrin-mediated uptake. *J. Cell Biol.* **158**, 1119-1131 (2002).
81. Gobeil, L. A., Lodge, R. & Tremblay, M. J. Macropinocytosis-like HIV-1 internalization in macrophages is CCR5 dependent and leads to efficient but delayed degradation in endosomal compartments. *J. Virol.* **87**, 735-745 (2013).
82. Watarai, M., Makino, S., Fujii, Y., Okamoto, K. & Shirahata, T. Modulation of Brucella-induced macropinocytosis by lipid rafts mediates intracellular replication. *Cell. Microbiol.* **4**, 341-355 (2002).
83. Brandt, W. E., McCown, J. M., Gentry, M. K. & Russell, P. K. Infection enhancement of dengue type 2 virus in the U-937 human monocyte cell line by antibodies to flavivirus

cross-reactive determinants. *Infect. Immun.* **36**, 1036-1041 (1982).
84. Littaua, R., Kurane, I. & Ennis, F. A. Human IgG Fc receptor II mediates antibody-dependent enhancement of dengue virus infection. *J. Immunol.* **144**, 3183-3186 (1990).
85. van der Schaar, H. M., Wilschut, J. C. & Smit, J. M. Role of antibodies in controlling dengue virus infection. *Immunobiology* **214**, 613-629 (2009).
86. Diamond, M. S., Edgil, D., Roberts, T. G., Lu, B. & Harris, E. Infection of human cells by dengue virus is modulated by different cell types and viral strains. *J. Virol.* **74**, 7814-7823 (2000).
87. van der Schaar, H. M. *et al*. Characterization of the early events in dengue virus cell entry by biochemical assays and single-virus tracking. *J. Virol.* **81**, 12019-12028 (2007).
88. Ayala-Nunez, N. V., Wilschut, J. & Smit, J. M. Monitoring virus entry into living cells using DiD-labeled dengue virus particles. *Methods* **55**, 137-143 (2011).
89. Vonderheit, A. & Helenius, A. Rab7 associates with early endosomes to mediate sorting and transport of Semliki forest virus to late endosomes. *PLoS Biol.* **3**, e233 (2005).

Supplemental Information

Supplemental Figures

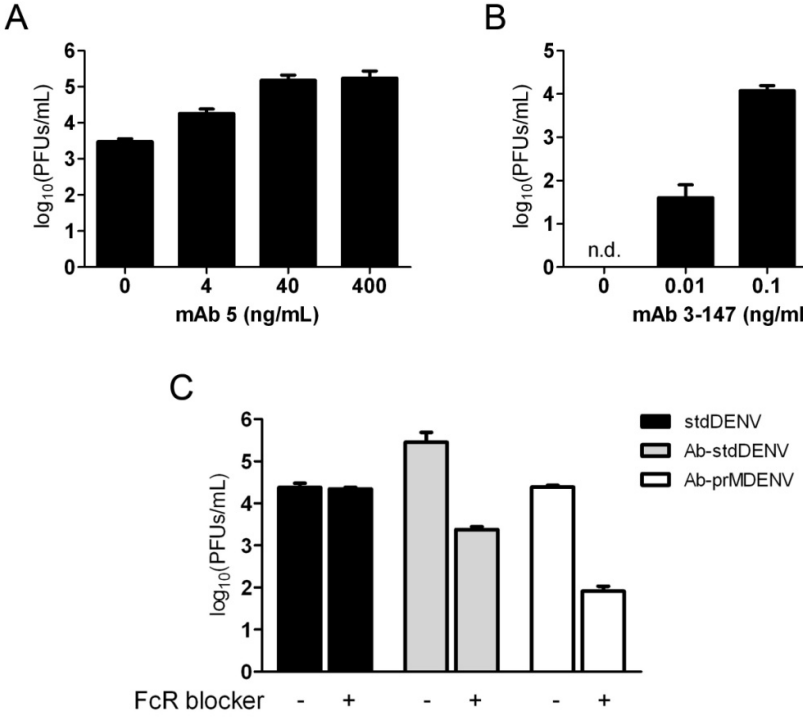

Figure S1. Anti-E and anti-prM antibodies enhance DENV infection via FcγRs. (A) Enhancing profile of anti-E mAb 5 complexed to stdDENV in P388D1 cells. **(B)** Enhancing profile of anti-prM mAb 3-147 complexed to prMDENV. Virus particle production was assessed at 43 hours post-infection by plaque assay. **(C)** DENV particle production in cells treated with and without FcR blocker. Bars represent the average of three independent experiments ± SEM.

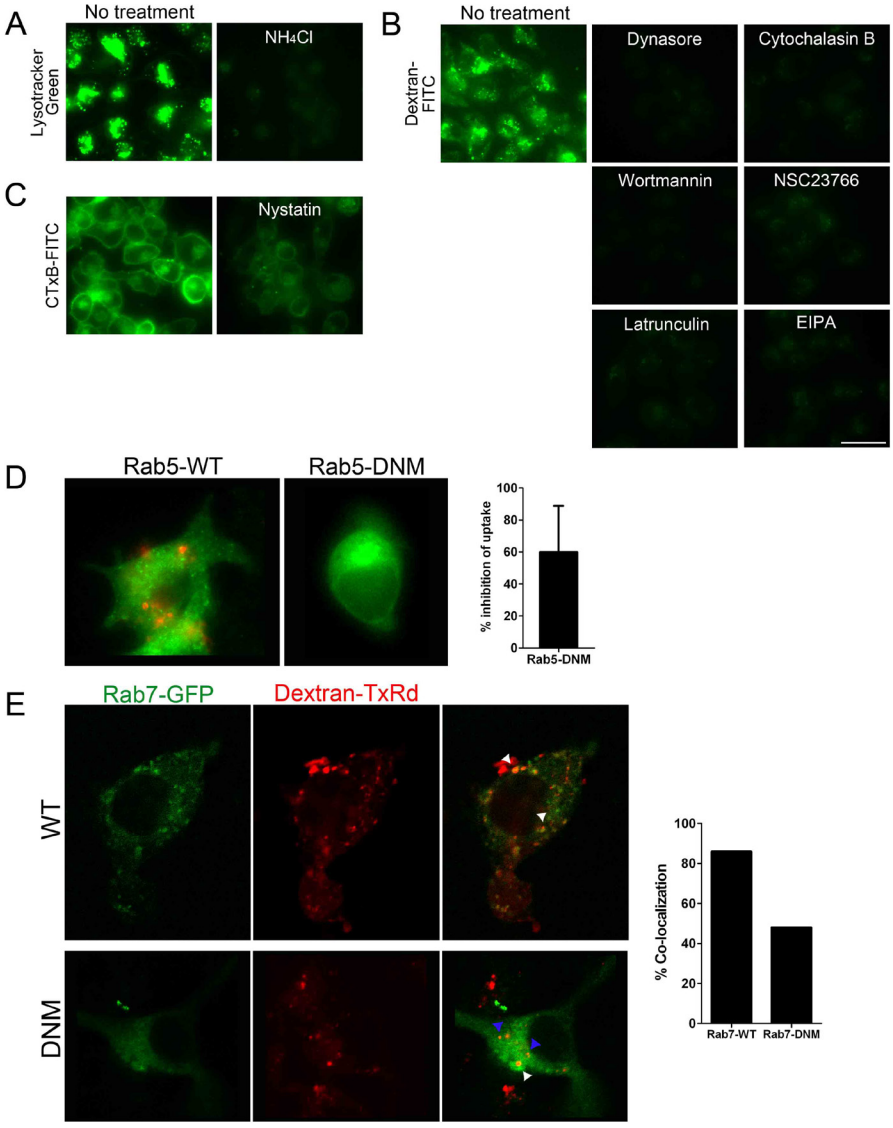

Figure S2. Fluorescently labeled cargo controls used to confirm the activity of different biochemical inhibitors and Rab5 and Rab7 DNM constructs. The cargo controls were added to P388D1 cells upon treatment with biochemical inhibitors. **(A)** Lysotracker Green was used for ammonium chloride (50 mM), **(B)** Dextran-FITC for dynasore (150 μM), cytochalasin B (15 μM), latrunculin (1 μM), wortmannin (2 μM), NSC23766 (250 μM), and EIPA (100 μM), and **(C)** CTxB-FITC for nystatin (50 μM). Scale bar: 25 μm. **(D)** Dextran-TxRd was added to P388D1 cells after electroporation with Rab5 or Rab7 plasmids (GFP-tagged WT and DNM). The activity of the Rab5-DNM was assessed by quantifying Dextran-TxRd uptake in the DNM and WT cells. To this end, 50 cells were used of each condition. The percentage of inhibition of uptake of the DNM was calculated with respect to the WT plasmid control. **(E)** The activity of the Rab7-DNM was defined by quantifying co-localization of Dextran-TxRd molecules and Rab7-GFP+ compartments. The white arrowheads indicate examples of co-localization. The blue arrowheads show examples of what was scored as no co-localization. The graphs shows co-localization results of 50 Dextran molecules per condition.

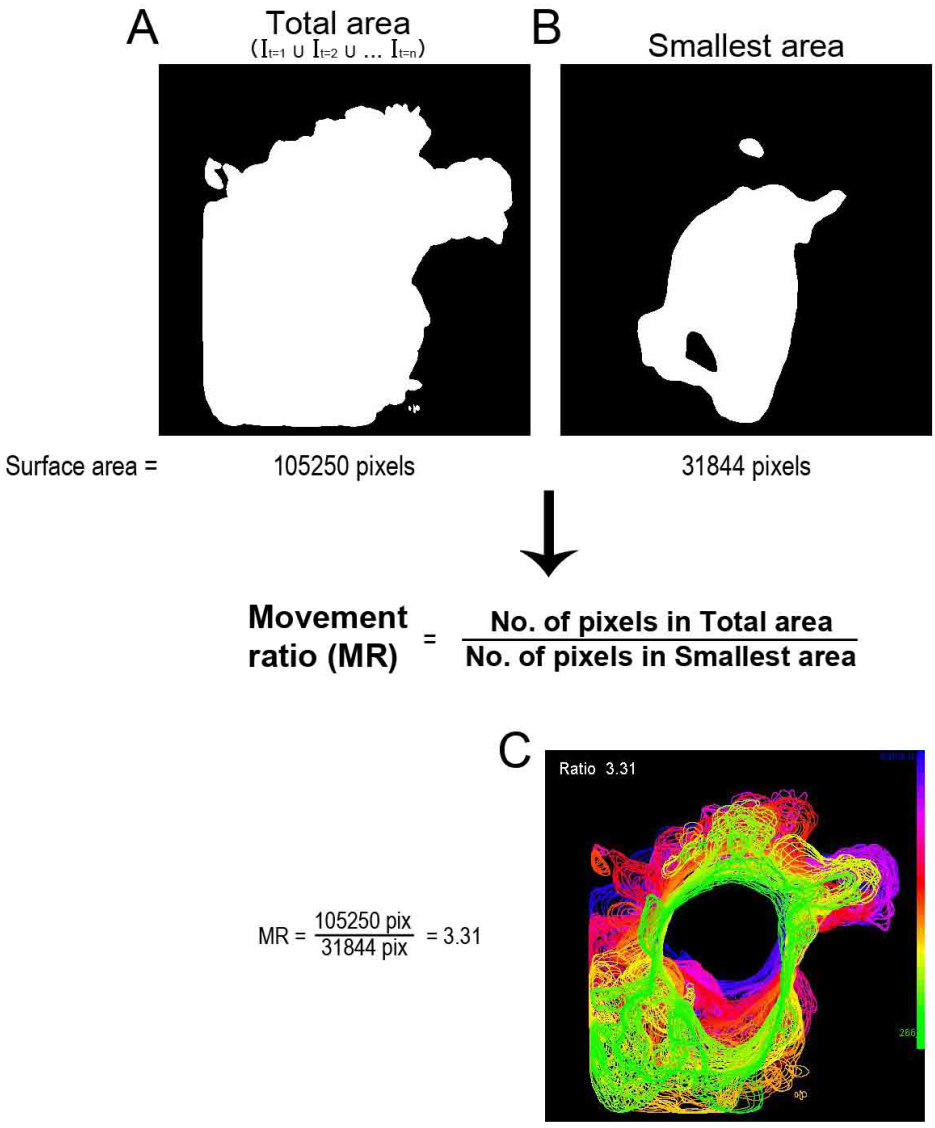

Figure S3. How to calculate the "Movement ratio" (MR). The Movement ratio quantifies the extent of movement of one cell over a frame sequence. To calculate it, images from the sequence are thresholded (binarized) to identify the pixels occupied by the cell at each frame. **(A)** The "total area" covered by the moving cell for the whole sequence is obtained by counting all pixels in the union of these binarized frames. **(B)** The area occupied by the cell before movement starts (smallest area) is obtained from the binarized frame with the smallest number of pixels. Finally, the MR in the image sequence is quantified by the ratio of the pixels obtained in **(A)** and **(B)**, where 1 corresponds to immobility and higher numbers correlate with higher cell mobility. In this example, we used a sequence of 266 frames. **(C)** Overlay of the cell body outlines of the same time-lapse. The colors indicate time direction. The whole procedure was done with ImageJ.

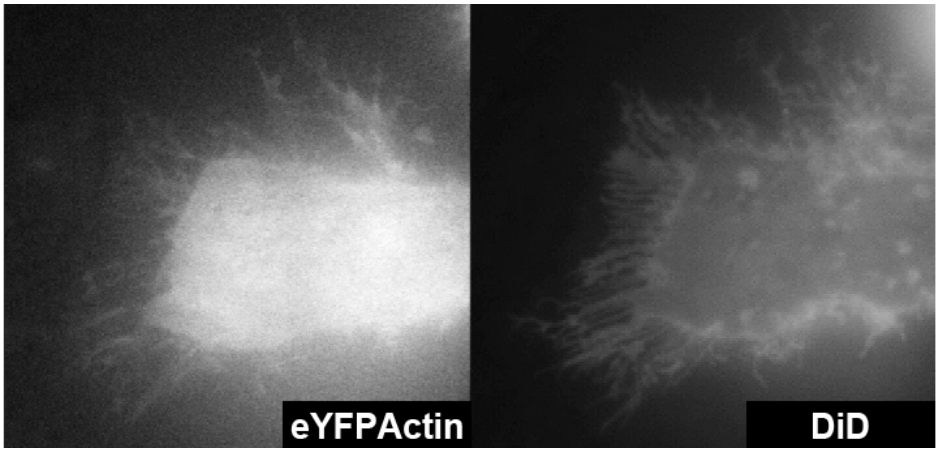

Figure S4. Overlap of eYFPActin expression and DiD-labeling of cytoplasmic membrane. P388D1 cells electroporated with eYFP-Actin were stained with the lipophilic probe DiD for 1 h at 37ºC. DiD was incorporated on the cell membrane. The cells were washed and imaged with an epi-fluorescence Leica Biosystems 6000B microscope. As shown in the figure, the DiD signal overlaps with eYFP-Actin.

Movie legends

Movie S1. Single-particle tracking of Ab-stdDENV particle in P388D1 cells. DiD-labeled stdDENV particles were opsonized with mAb5 and added *in situ* to the cells. The movie was recorded at a time-lapse of 1 frame per second using an epi-fluorescence Leica Biosystems 6000B microscope. A sequence of 70 frames is shown. Membrane fusion is evident as a sudden increase in DiD fluorescence intensity. The images were artificially modified to show the differences in fluorescence intensity, from low intensity (purple) to high intensity (yellow).

Movie S2. Extensive ruffling induced by Ab-stdDENV. Actin-eYFP expressing P388D1 cells were infected with DiD-labeled Ab-stdDENV. The cells were then imaged with a Solamere Spinning Disk Confocal Live Cell Imaging system at 1 frame per 4.5 seconds with a 63x objective. Shown is a sequence of 300 frames. For clarity, the DiD channel is not shown.

Movie S3. Extensive ruffling induced by Ab-prMDENV. Actin-eYFP expressing P388D1 cells were infected with DiD-labeled Ab-prMDENV. Imaging was performed as described to the legend of Movie S2. A sequence of 400 frames is shown. The DiD channel is not shown for clarity purposes.

Movie S4. Mock-infected P388D1 cells. Actin-eYFP expressing P388D1 cells were incubated with HNE buffer and imaged as described to the legend of Movie S2. A sequence of 250 frames is shown.

Movie S5. Cells before Ab-DENV induced extensive ruffling. Actin-eYFP expressing cells were infected with DiD-labeled Ab-prMDENV. Imaging was performed as described to the legend of Movie S2. The movie shows the first minutes following infection.

Movie S6. Cells after Ab-DENV induced extensive ruffling. Actin-eYFP expressing cells were infected with DiD-labeled Ab-prMDENV. Imaging was performed as described to the legend of Movie S2. The movie starts at 4.5 mpi. A sequence of 160 frames is shown.

Movie S7. Macropinosome closure and internalization. Actin-eYFP expressing cells were infected with DiD-labeled Ab-stdDENV. Imaging was performed as described to the legend of Movie S2. A sequence of 140 frames is shown.

Movie S8. Macropinosome closure and internalization. Actin-eYFP expressing cells were infected with DiD-labeled Ab-stdDENV. Imaging was performed as described to the legend of Movie S2. A sequence of 100 frames is shown.

Movie S9. Example of Type 2 uptake. Actin-eYFP expressing P388D1 cells were infected with DiD-labeled Ab-prMDENV. Imaging was performed as described to the legend of Movie S2. A sequence of 16 frames is shown.

Movie S10. Example of a multiple Type 2 uptake attempts to capture the virion. Actin-eYFP expressing P388D1 cells were infected with DiD-labeled Ab-stdDENV. Imaging was performed as described to the legend of Movie S2. A sequence of 300 frames is shown.